ACADEMIC PRESS

Available online at www.sciencedirect.com

SCIENCE DIRECT®

Journal of Sound and Vibration 260 (2003) 67–82

JOURNAL OF SOUND AND VIBRATION

www.elsevier.com/locate/jsvi

Indicated repeatable runout with wavelet decomposition (IRR-WD) for effective determination of bearing-induced vibration

S. Vafaei, H. Rahnejat*

Wolfson School of Mechanical and Manufacturing Engineering, Loughborough University, Loughborough, UK

Received 18 December 2000; accepted 4 March 2002

Abstract

Bearings are often the limiting factors for performance of rotor systems. There are various sources that contribute to rotor vibration due to bearing elements. These include the variable compliance effect, spinning and sliding motions of rolling elements, manufacturing anomalies in the form and finish of bearing elements and the out-of-centre assembly of shafts on bearing supports. Therefore, the signature of vibration is quite complex and its decomposition into its constituent contributory factors can be significant in fault diagnosis and for remedial actions. This paper highlights a novel method for acquisition of real-time vibration signature of rotor systems, based upon the decomposition of the indicated repeatable runout for synchronous components of vibration. It is shown that wavelet analysis can be employed to reduce the burden of long-record data manipulation. The methodology is termed "indicated repeatable runout with wavelet decomposition".

1. Introduction

A vibration spectrum is referred to as a mechanical signature, and the determination of information from it, is referred to as signature analysis. Traditionally, mechanical signatures are obtained from known "healthy" machines, as the standard. Signatures taken at later occasions can be compared with the standard and significant changes noted, leading to corrective actions to be undertaken. Ideally, the signature components or contributions can be attributed to specific causes (i.e., mechanical parts), in order to facilitate for specific remedial actions. Therefore, impending failures can be predicted. In order to achieve this aim, an analytical model for

*Corresponding author. Tel.: +44-1509-227569; fax: +44-1509-227569.
E-mail address: h.rahnejat@lboro.ac.uk (H. Rahnejat).

0022-460X/03/$ - see front matter
PII: S0022-460X(02)00900-8

prediction of various contributory factors should be developed and a signal decomposition technique devised in order to analyse the real-time data. Cross-correlating these two approaches should point to the causes of vibration and their contribution.

Diagnosing the contributing factors to rotor vibration, such as out-of-balance, misalignment, and manufacturing defects, as well as wear- and fatigue-induced pits and cracks, would play an important role in reducing operation and maintenance costs [1]. This task is usually achieved through vibration monitoring and signal processing in the time domain such as decomposition wavelet transform or in the frequency domain such as by fast fourier transform (FFT), auto-regressive (AR) method and auto-regressive moving average method (ARMA).

Among the various contributory factors to bearing vibration, out-of-balance vibration is usually the most prominent. This can be attributed to a variety of causes, such as eccentric assembly of rotors to bearing supports, out-of-roundness of the bearing rings or the excursion of the shaft centre away from the centre of the bearing due to the mutual convergence and divergence of bearing rings under dynamic conditions. This is often as a result of loss of preload. Therefore, out-of-balance rotation is often the most commonly encountered problem. Rotor imbalance not only causes an increase in the radial force, but also an increase in the axial force in a proportionate manner, where angular contact bearings are employed [1]. This paper, therefore, is based upon the determination of the synchronous runout component of spindle vibration under strictly controlled experiments. The effects of the most likely contributory factors have been studied in some detail.

The primary out-of-balance vibration occurs at the apparent rotor speed (i.e., the shaft frequency), therefore, it is referred to as synchronous whirl. Superimposed upon this are other synchronised events as multiples of the same frequency, related to the bearing elements' relative speeds (see Section 4) [2–4]. The total indicated runout (described in Section 2) is due to the overall contribution of these effects, as well as being due to non-synchronous events. The decomposition of these at an instant of time leads to the determination of all contributions and facilitates a snapshot of the prevailing conditions. This paper proposes a new scheme for detecting the spindle imbalance, based on an average method and a time decomposition wavelet transformation.

2. Signal processing method

2.1. Indicated repeatable runout with wavelet decomposition (IRR-WD)

It is shown in Section 2.3 that when an average is taken in an increasing sequence of signals, the non-repeatable contributions in the sequence gradually diminish. This is demonstrated in Fig. 1. When the averaging process is applied in the domain of signal 2, signal 1 remains repeatable, whilst signal 3 becomes non-repeatable and its contribution diminishes with an appropriate choice of sequence (i.e., a sufficient number of samples in the averaging process). Consequently, the effect of signal 2 and all other contributions at higher frequencies such as the case for signal 1 remain.

This technique can be employed to window around a region of interest. For instance, if the effect of out-of-balance at a shaft frequency of 100 Hz is desired, one may use the technique to initially include all contributions at and above 105 Hz as well as at and above 95 Hz. The subtraction of the two waveforms results in the isolation of all the repeatable runout (RRO)

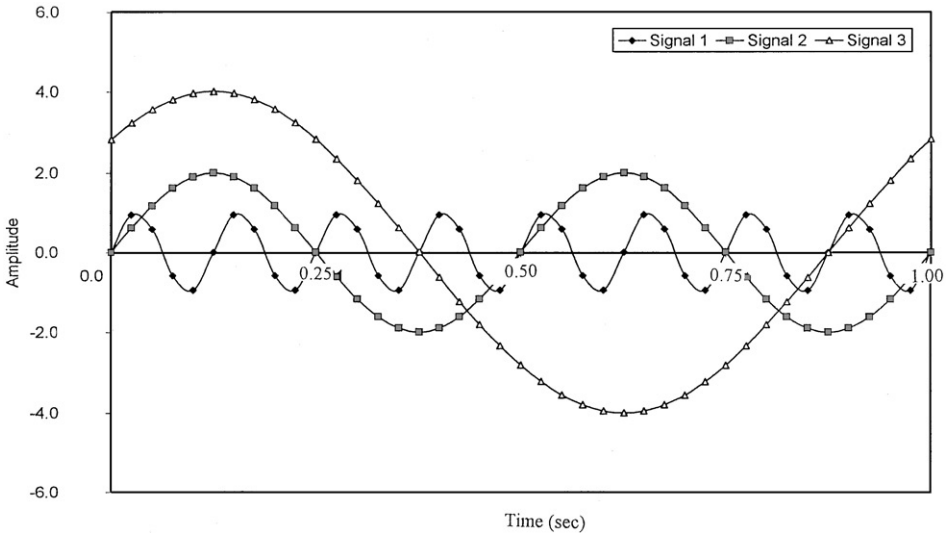

Fig. 1. The diminishing nature of the averaging process for a non-repeating sequence.

contributions for the band of frequencies 95–105 Hz. In effect, a windowing method has been devised for time domain analysis. Therefore, the IRR process may be considered to behave rather like a band pass filter, although this is not exactly the case, as the subtraction of repeatable frequencies occur relative to the averaging frequencies in the chosen range. Therefore, the process used is based on the traditional averaging method, but in the time domain to represent a spatial frequency range of interest. The method is very simple, but almost exact if the prior knowledge of an existing frequency exists, such as bearing-induced contributions. The important issue is to ensure that the intended isolated frequency has a repeatable waveform within the chosen band. The remaining signal, after the completion of the process, contains a host of repeatable frequencies within the chosen range (i.e., 95–105 Hz in this example). However, when one is seeking the contributions at a given frequency (e.g., at the out-of-balance frequency of 100 Hz), it is necessary to decompose the remaining signal further to obtain the desired contribution. This has been achieved through application of wavelet analysis, after the 'averaging' process has been completed (see Section 2.3).

A particular advantage of this method is the elimination of all other frequencies with increasing number of samples and multitude of employed sequences. Whilst, in theory, this can be easily proven to be the case [5], in practice and with complex bearing vibration, a large sequence of samples with a large number of data points may be required. In order to minimise the formidable data handling requirements, one may resort to wavelet decomposition (as described above, and in Section 2.3) as an integral part of this process. Therefore, subsequent wavelet transformations can be undertaken in the case of bearing vibration. For example, for the shaft frequency of 120 Hz, the number of samples used in the analyses carried out in this study is typically 120, each with 2184 data points.

2.2. The averaging method in TIR

When the TIR is sampled with L equal sector data per a rotor revolution, and measured for M revolutions, then TIR (l, m) can be defined as the total indicated runout, corresponding to the first sector for the mth revolution.

The RRO is independent of m, because it is repeated in each revolution, so that TIR can be written as follows:

$$TIR(l,m) = RRO(l) + NRRO(l,m). \tag{1}$$

RRO can be obtained by averaging TIR in each sector, assuming that the non-repeatable (NRRO) is a stationary random variable of mean zero for a large number of data points. Thus

$$\frac{1}{M}\sum_{m=1}^{M} TIR(l,m) = \frac{1}{M}\sum_{m=1}^{M}(RRO(l) + NRRO(l,m)) \approx RRO(l). \tag{2}$$

Substituting for the above equations, NRRO can be obtained by subtracting RRO and the average of TIR from the instantaneous TIR [5], as

$$NRRO(l,m) = TIR(l,m) - \frac{1}{M}\sum_{m=1}^{M} TIR(l,m). \tag{3}$$

The runout is divided into synchronous and non-synchronous components, with each component further subdivided into two parts, the stationary and the random contributions [6] (see Table 1):

2.3. wavelet analysis

The original idea for wavelet decomposition is now more than half a century old. However, only in recent times have systematic applications been undertaken and the method has begun to be established [7–9].

The development of new wavelet bases has enabled the construction of algorithms for differential and integral equations, which are more efficient than the earlier algorithms [10]. Wavelet analysis decomposes a given signal into its components, which are not necessarily simple harmonic functions, as is the case in Fourier analysis. Wavelets can be functions of different possible families of orthogonal local basic functions [11,12]. Wavelets provide a new tool for the analysis of vibration records. They allow the changing spectral composition of a non-stationary signal to be measured and presented in the form of a time–frequency map [13]. Wavelet analysis involves a fundamentally different approach. Instead of seeking to break down a signal into its

Table 1
The classification of rotor runout

Synchronous		Non-synchronous	
Stationary	Random	Stationary	Random
RRO		NRRO	

harmonics, which are global functions that go on forever, the signal is broken down into a series of local basic functions called wavelets. Each wavelet is located at a different position on the time axis and is local in the sense that it decays to zero, when it is sufficiently far from its centre. At the finest scale, wavelets may be very short indeed, whilst at a coarse scale, they may be very long [12,13].

The time–frequency distribution obtained through a wavelet transform enables one to observe the contribution of different frequency components over the full spectrum from one instant to the next. Obviously, the aforementioned time variations due to bearing defects would appear at frequencies near the resonant frequencies, excited by for example an impact upon a bearing defect [1,2,14].

It is possible to decompose any arbitrary signal $f(x)$ into its wavelet components. The approach is the same as for harmonic analysis except that, instead of breaking a signal down into harmonic functions of different frequencies, the signal is broken down into wavelets of different scale (different level) and different positions along the x-axis. A finite length known signal $f(x)$, occurring over the interval $0 \leqslant x < 1$ can be represented as a constant level (i.e., for all the wavelets of level less than zero) plus wavelets of all levels above zero. Thus

$$\begin{aligned} f(x) = {} & a_0 + a_1 w(x) \\ & + a_2 w(2x) + a_3(2x-1) \\ & + a_4 w(4x) + a_5 w(4x-1) + a_6 w(4x-2) + a_7 w(4x-3) \\ & + a_8 w(8x) + a_9 w(8x-1) + a_{10} w(8x-2) + \cdots, \end{aligned} \tag{4}$$

where

$$f(x) = a_0 + \sum_{j=0}^{\infty} \sum_{k=0}^{2j-1} a_{2^j+k} w(2^i x - k), \quad 0 \leqslant x < 1. \tag{5}$$

The discrete wavelet transform (DWT) is an algorithm for computing a_0, a_{2^j+k}, when $f(x)$ is sampled at equally spaced intervals over $0 \leqslant x < 1$. The DWT algorithm was initially devised by Mallat [15] and is often referred to as the Mallat's pyramid algorithm or the Mallat's tree algorithm. For detailed information about wavelet transformation, readers are referred to Refs. [8,10–13,15].

The wavelet decomposition tree can yield valuable information, depending upon the shape of the wavelet used. The selection of wavelet is important in the wavelet analysis. There are an infinite number of possibilities for this, but only a small subset of these meets the conditions that are necessary if the wavelets are to give an accurate decomposition and remain orthogonal to each other. Therefore, in order to obtain a smoother function, it is necessary to include more terms in the wavelet shape function.

A signal subjected to the IRR process contains contributions within the chosen frequency range, which can be referred to as a "window". To obtain the contribution at a specific desired frequency, one would need to decompose the remaining signal further. This is where the use of wavelet comes to its own. The analysis used in this study uses the wavelet form "db10" [8]. The waves related to the bearing contributions are quite smooth and it has been found that the orthogonal db10 wavelet works ideally in such cases. Therefore, the wavelet is merely used to decompose the repeatable frequency in the chosen range, without interfering with the other

components or contributions in the original signal. The reason for this approach is the insufficient data record in the original signal to eliminate noise and non-repeatable contributions. Should sufficient number of samples exist, the need for wavelet decomposition is eliminated.

3. The experimental investigation

3.1. The experimental apparatus

An experimental rig is devised to investigate the vibration spectra of a high-speed precision 7.5 kW power routing spindle (see Fig. 2). This type of vertical spindle is used in routing wood composites and non-ferrous materials, including some highly abrasive and hard work-piece materials used in the aerospace industry. The spindle speed, depending on application, varies from 1000 to 28,000 r.p.m. (usually in the range 12,000–28,000 r.p.m.) with a table feed rate in the range 5–15 m/min under dry cutting condition. In order to minimize the sources of vibration, the spindle

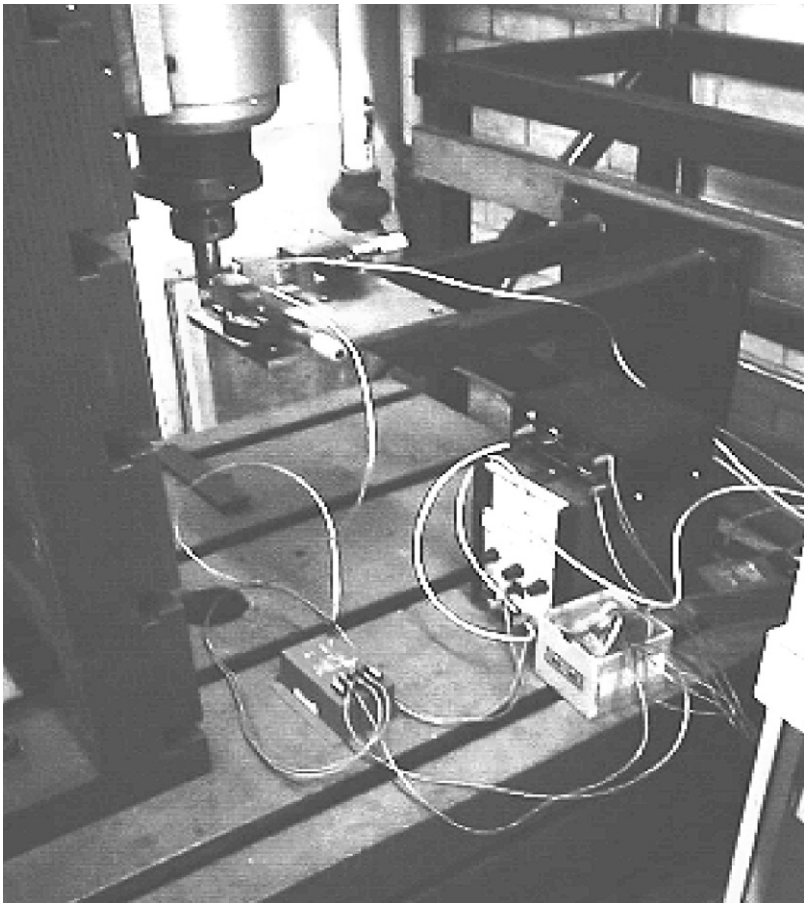

Fig. 2. The experimental rig.

is configured as a non-contact drive system, where the rotor is supported by pairs of angular contact ball bearings in a tandem arrangement at each end and in a back-to-back formation, providing a high dynamic stiffness. The bearings are grease lubricated for spindle speeds up to 20,000 r.p.m. and oil lubricated for spindle speeds up to 28,000 r.p.m. In this study a grease lubricated bearing arrangement is employed. The purpose of the study is to monitor spindle vibration in the free running (i.e., no cutting action) of the spindle with the purpose of identifying the vibration spectrum produced by ball bearings.

Under the spindle free running condition, the system is subjected to a pre-determined axial pre-load and a suitable radial interference fit to the rotor. Therefore, the main sources of vibration are due to imperfections on rolling elements' and raceways' surfaces, as well as the bearings' variable compliance effect and any out-of -balance in the spindle assembly. For the purpose of this investigation, the spindle is mounted on a cast iron pedestal which is in turn attached firmly to a heavy cast iron machine bed. Cast iron structures are used, because of their damping characteristics caused by structural porosity . The large mass of the assembly, fixed rigidly to a concrete foundation, places its natural modal frequencies considerably above the frequencies of generated vibration [4,16].

3.2. Spindle bearings

There are two sets of angular contact ball bearings in tandem at each end of the spindle, set in a back-to-back arrangement. This provides good dynamic stiffness and thrust load carrying capacity in the vertical axial direction. A spacer is placed between the pairs of bearings to effect the transfer of an axial pre-load of 700 N. The tandem set of bearings, nearer to the position of the tool (referred to as the tool-end bearings), are fixed in location, whilst the other pair of bearings at the "free-end" of the rotor are allowed to axially float. The detail specification of these bearings is given in Table 2.

The angular contact ball bearings can withstand medium to high axial loads and medium radial loads, thus providing an excellent moment capacity.

3.3. Sensors and data acquisition system

Vibrations in this free spindle running arrangement are monitored in the horizontal radial plane (i.e., in the X and the Y directions if Z is considered to be the spindle's vertical axial direction).

Table 2
Angular contact ball bearing specification

	Free-end bearing	Tool-end bearing
Ball diameter	7.144 mm	7.144 mm
No. of balls	11	12
Contact angle	15°	15–16°
Pitch diameter	33.5 mm	46 mm
Bore diameter	25 mm	35 mm
Inner race diameter	26.345 mm	38.845 mm
Outer race diameter	40.654 mm	53.154 mm

Specially configured non-contacting eddy current probes are used to monitor vibrations in the radial transverse XY plane. Each probe is mounted in a precision sliding jig mounted upon a plate, isolated by 20 mm thick serrated neoprine pads from the long arms that are mounted to a separate rigid structure which is in turn fixed to a solid wall (see Fig. 2). It can be observed that in this arrangement the sensor- carrying structure is isolated from the foundation upon which the rig itself is mounted.

The eddy current probes are configured in order to provide a high measurement resolution, providing a 40 mV full scale output for 1 μm displacement of the spindle in X or Y directions. The probes are driven in position by high-resolution digital micrometers to the vicinity of a highly polished and heat treated test piece mounted in the spindle collet.

The positioning of the probes is a critical factor in the acquisition of a coherent signal, which is dependent upon an "optimum" distance from the test-piece surface. In this application, a gap of 100–150 μm is found to be ideal and is maintained.

The sensor output after appropriate filtration to eliminate unwanted noise and static voltage is fed to a 12 bit 16 channel 1 MHZ data acquisition board.

4. The analytical method

The inherent primary frequencies generated by bearings in any dynamic structure, which is supported by ball or rolling elements, are related to the bearing geometry. Out-of-balance contributions at the shaft rotational frequency, f_s, is always evident in any rotor-bearing assembly system, as various sources contributing to unbalanced rotation of shafts cannot be practically avoided. These include out-of-roundness of bearing rings or eccentricity between the centre of rotation of rotor and the support bearings' geometric centre.

Expressions for other well-known bearing contributions have been obtained and are listed below [1,2,4,16]:

(i) Cage frequency:

$$f_c = \frac{f_s}{2}\left(1 - \frac{d\cos\alpha}{D}\right). \tag{6}$$

(ii) Ball passage frequency (ball to outer race frequency):

$$f_{bo} = Nf_c. \tag{7}$$

(iii) Ball to inner race frequency:

$$f_{bi} = \frac{Nf_s}{2}\left(1 + \frac{d\cos\alpha}{D}\right). \tag{8}$$

(iv) Ball frequency:

$$f_b = \frac{Df_s}{2d}, \tag{9}$$

where N is the number of balls, D is the pitch circle diameter, d is the ball diameter and α the contact angle.

In addition to the above, manufacturing defects in form and finish of rolling elements and raceway surfaces induce other untoward motions. Wardle [2], Rahnejat and Gohar [17] and Aini et al. [3] deal with these features in their investigations of bearing induced vibration. These contributions occur as the result of perturbations in the dynamic rolling element to races reactions that take place over and above the changes due to the balls entering and leaving the loaded and unloaded regions of the bearing, caused by the mutual convergence and separation of the bearing rings. These perturbations can occur as the result of waviness of bearing rings, "off-sized" balls or rolling elements as discussed by Meyer et al. [18].

In the response region of interest (0–2 kHz), surface waviness of bearing raceways produce sideband frequencies at $\pm nf_s$ (where n indicates multiples of the shaft speed) with respect to the principal frequencies that are the harmonics of the ball pass rate Nf_c. Waviness of balls and raceways account for most of the large amplitude imperfections that may occur in a ball bearing. "Off-sized" balls also contribute to bearing vibration owing to reduced radial gap size or larger elastic deflections. This contribution occurs at multiples of $j2f_b$. Therefore, sideband frequencies (as shown by Wardle [2]) can appear around the principal frequencies with the spacings of $f_s, f_c, 2f_b$. Therefore, the side-band frequencies due to bearing elements' waviness occur as the result of fluctuating contact reactions between interacting mating members (i.e., balls to inner and outer races' contacts). These are:

$$\text{outer race waviness} \pm \text{ball size} = iNf_c \pm jf_c \tag{10}$$

$$\text{outer race waviness} \pm \text{ball waviness} = iNf_c \pm j2f_b, \tag{11}$$

$$\text{outer race waviness} \pm \text{inner race waviness} = iNf_c \pm jf_s, \tag{12}$$

$$\text{inner race waviness} \pm \text{ball size} = iN(f_s - f_c) \pm f_c, \tag{13}$$

$$\text{inner race waviness} \pm \text{ball waviness} = iN(f_s - f_c) \pm j2f_b \tag{14}$$

for $i = 1, m$ and $j = 1, n$

At the first glance, the recognition of the various frequency peaks within the spectrum of vibrations appears to be a daunting task. However, using the methodology outlined above this task becomes somewhat less laborious.

It can be observed that the acquired vibration signals from such spindles contain many contributions from bearing-induced vibration. As shown by the above "idealised" analytical model, there are a host of interactions such as waviness on rolling contact surfaces. The significant contributions from bearing-induced vibration are speed dependent, thus repeatable within a spatial window. This fact enables the use of the methodology described in Section 2. However, to include all the effects the record length should correspond to the highest contributions, which are usually as the result of secondary bearing vibrations. This results with a shortage of sampled data at the lower primary bearing frequencies, thus making the use of wavelets necessary, as described in Section 3.

5. Results and discussion

The methodology in Section 2 is applied to the experimentally obtained signals. The apparent spindle speed was kept at 7200 r.p.m. (i.e., shaft frequency of 120 Hz). The frequencies employed for the wavelet decomposition were 115–125 Hz, respectively. This was carried out after successive application of IRR-WD method. The period of oscillations corresponding to the shaft frequency is approximately 8.33 ms. Results obtained, after the completion of the process, are shown in Fig. 3(a). Note that the waveform corresponds to all the frequencies in the band 115–125 Hz. With the only significant contribution, being the shaft frequency in this region, one can consider the waveform to indicate the runout at the synchronous whirl. The harmonic nature of the response is as expected, the amplitude of which is the contribution of shaft out-of-balance rotation to the overall vibration signal (approximately 0.4 μm). The steady component (this being the deviation from an average zero position) of the out-of-balance can be measured as the difference between the peak-to-valley amplitudes. It can be noted that this value is quite small, though not zero. The small value in the region of tens of nanometers is expected, as this result is for the case of a nominally balanced spindle and tool-piece assembly.

The same procedure can be applied to obtain results at other synchronous contributions. These include vibrations induced by cage, as well as by balls relative to the inner and outer raceways in addition to ball–spin. Figs. 3(b)–(e) show the results at cage, ball–spin, ball-to-inner and ball passage frequencies, respectively. Note that in Fig. 3(b), vibration due to cage oscillations is merely $< \pm 0.1$ μm, and has the expected quasi-harmonic variation. In Fig. 3(c), the contribution due to ball frequency is of the same order as for the shaft frequency. The waveform is marginally asymmetric with a period of 3.2 ms, with the first half of the cycle being shorter in duration. This indicates slip during that period, corresponding to a shorter traverse time than the expected half-period. This is confirmed by the oscillations in Fig. 3(d) for the ball-to-inner relative speed, with a period of 13.8 ms. Note that due to slip, the point on the time axis occurs before the expected half-cycle period. This confirms slipping of the ball relative to the inner race and is in concordance with the ball–spin conditions shown in Fig. 3(c).

Fig. 3(e) shows the contribution at the ball passage frequency (i.e., ball-to-outer relative speed). This effect is also known as the variable compliance effect, indicating vibration caused by the dynamic stiffness variation as the ball complement repeats its orbital disposition. In other words, between consecutive repeating orbital formations the system's effective stiffness alters. With a stationery outer race, the period due to the ball passage frequency corresponds to the time taken for a ball to traverse the circumferential distance between any pair of successive balls. This period is approximately 1.9 ms. During this period, the balls may enter or depart from the loaded region of the bearing, created by the rotating out-of-balance force. Referring to Figs. 3(a) and (e) one can observe that as the ball complement is being displaced in its orbital path, the shaft centre goes through approximately a quarter of its cycle. Therefore, balls can be subjected to loading and unloading at least 4 times during each cycle of repeating stiffness. Whenever, a ball is subjected to increased loading the tendency to slip is diminished, whilst with reduced loading, emerging diametral clearances occur that increase the propensity to slip. In Fig. 3(e), the first half of the cycle shows an increased traverse time due to slip, whilst the latter part of the cycle corresponds to mutual convergence of rings. These results corroborate the findings in Figs. 3(c) and (d).

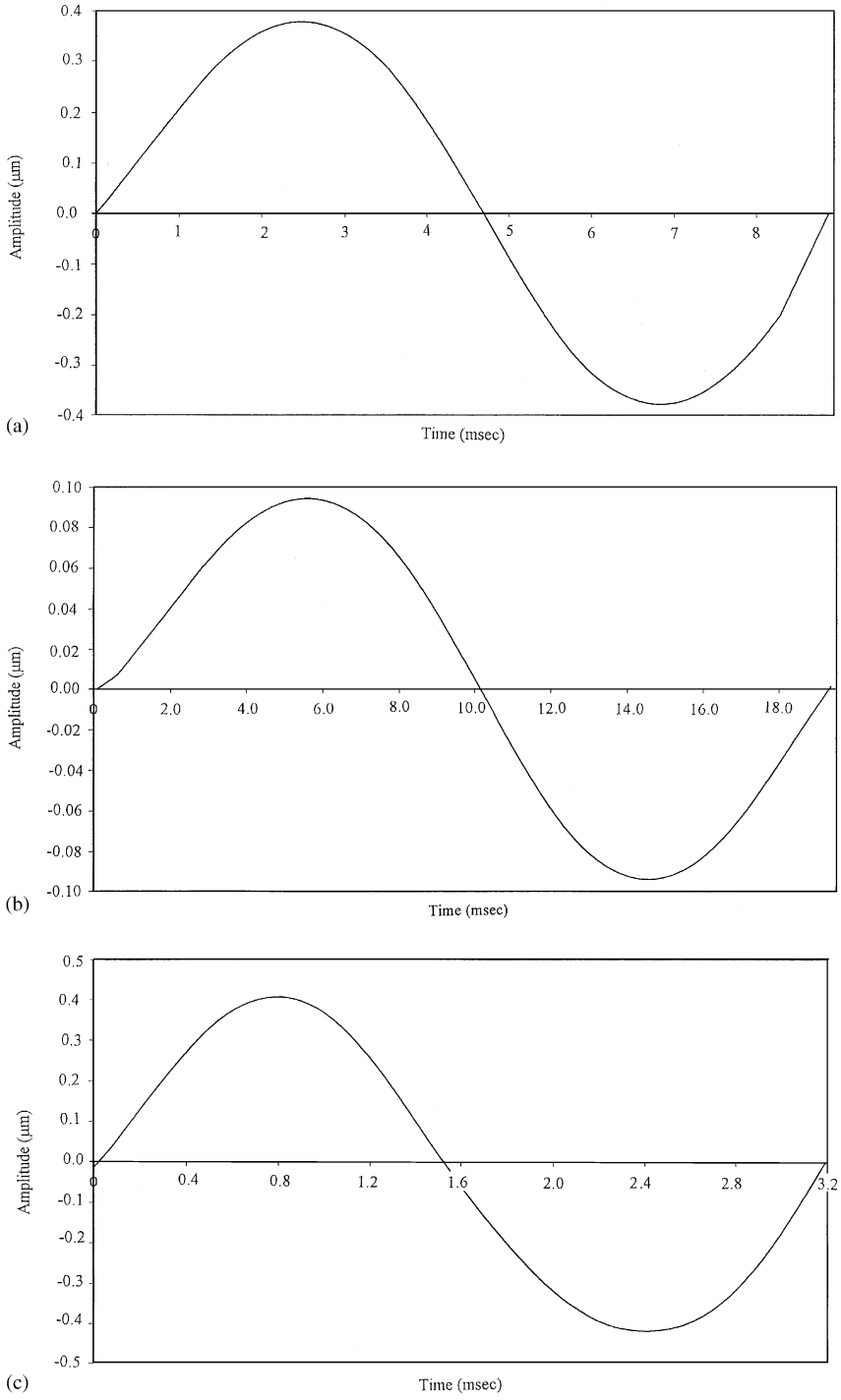

Fig. 3. The waveform (a) at the shaft speed, (b) at the cage speed, (c) due to ball-spin, (d) due to balls-to-inner race relative speed and (e) the variable compliance effect at the ball passage frequency.

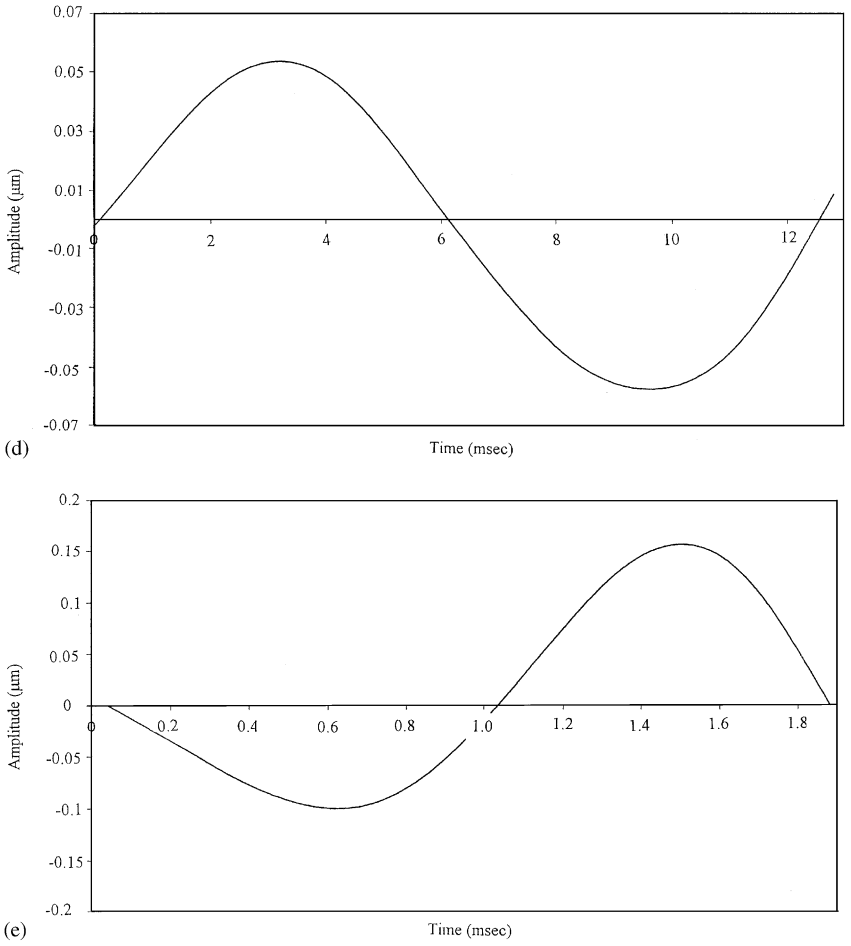

Fig. 3 (*continued*).

A practical problem, often encountered in industry, is the combined spindle–tool balance in routing and drilling operations. Routing tools are usually balanced separately by the tool manufacturer. The precision routing spindles are nominally balanced to within 5 μm. When tools are placed in the spindle collet, no further balancing action can be carried out, although provisions should be made for correct application of collet torque. It has been found that much of the untoward motions are due to inappropriate collet torques used by the operators in absence of a fool-proof device or proper guidelines. The investigation of this factor has led to the introduction of precise and typical out-of-balance here, in order to obtain optimum running conditions with this specific range of routing spindles under different speeds. The results presented here correspond to a speed of 7200 r.p.m. Different optimal running conditions emerge at various spindle speeds, indicating the complexity of the task in a multi-variate problem such as routing.

Fig. 4(a) shows the peak-to-valley lateral radial oscillations of the out-of-balanced spindle. Annuli of 100 g in mass are attached to the test piece. Each annulus has a displaced centre of mass

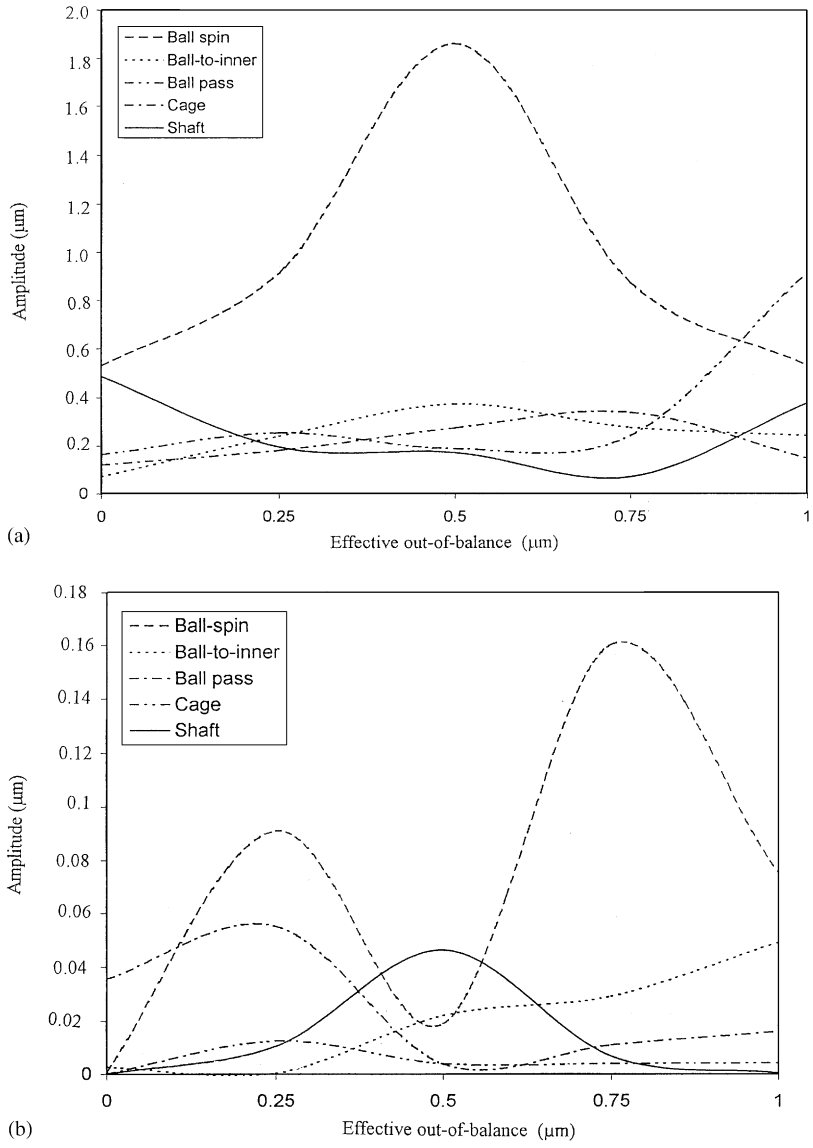

Fig. 4. (a) The effect of introduced out-of-balance on the bearing-induced vibrations and (b) the effect of out-of-balance on indicated runout at various bearing-induced contributions.

from the centre-line of the test piece by an amount indicated along the abscissa of the figure. Therefore, for example, when an annulus with a centre disposition of 1 mm is employed the total out-of-balance (excluding the nominal out-of-balance of the spindle and the tool) is regarded to be 100 g mm. This small out-of-balance is in fact quite significant, introducing an overall out-of-centre rotation in the region of 1–2 μm for the various annuli employed.

It can be observed that the peak-to-valley oscillations are significant at the ball frequency, f_b, and in-phase with the contribution at the ball-to-inner frequency, f_{bi}. The contribution at the cage

frequency, f_c, is also in-line with the same trend albeit with somewhat a phase lag. However, a reverse trend is observed for those attributed to the kinematic conditions for balls-to-the outer race contacts, f_{b0} and for the shaft out-of-balance motion, f_s, both of which indicate worsening conditions at higher values of the imposed out-of-balance. To understand the reasons for this phenomenon, one should obtain the runout contributions at these spectral components.

Referring to Fig. 4(b), it can be observed that optimal running conditions occur when the magnitude of the difference between the peak and valley oscillations is minimised. Such a condition corresponds to the minimisation of the steady component of the oscillatory behaviour (referred to as runout), whilst the actual double amplitude values (as in Fig. 4(a)) relate to the total transient excursions. This steady value indicates a bias in the eccentric position of the assembly. The results show that for the synchronous whirl at the shaft frequency, the conditions for the steady component oscillations worsen with the introduction of the annuli with values in the region: 50 gm mm (i.e., for a annulus with a 0.5 mm off-centre mass). The coincidence of this with the major contributory factor, f_b, in Fig. 4(a) indicates the presence of an off-sized ball that accounts for the major contributory factor, which also gives rise to the maximum cage response in the same figure. The fact that the runout contributions at the ball, ball-to-inner and the variable compliance effect do not coincide with the maximum shaft runout in Fig. 4(b) confirm the validity of the argument for an off-sized ball. Alternatively, the runout at the shaft frequency could only be physically explained by the eccentric rotation of the assembly, causing a significant contribution at the ball passage frequency due to the emergence of a defined circumferential loaded region. Referring to both Figs. 4(a) and (b) indicates this converse argument to be plainly untrue as both the transient excursions due to the variable compliance effect and the runout contribution due to the ball passage frequency remain insignificant at the maximum shaft centre runout. In fact the maximum indicated runout at f_{bo} is at 25 g mm out-of-balance, strongly affected by the ball–spin. It is clear that the main phenomenon, giving rise to spindle vibration here is a narrow loaded region event, caused by an off-sized ball, being approximately 1.9 μm over-sized.

6. Conclusions

A new signal processing method, based on the evaluation of synchronous runout has been developed and presented in this paper. A series of controlled experiments have been carried out in conjunction with the proposed method to determine the influence of bearing-induced vibration on the synchronous runout of a routing spindle-tool assembly. The signal processing method has found to be very effective in determining the individual vibration contributions related to the primary bearing-induced sources. The method; indicated runout (IR), requires a large number of samples at a high sample sizes. This necessitates the use of powerful computing machines. In order to eliminate the need for these, wavelet decomposition has been employed to effectively window around regions of interest with the IR method. The combination of the new method and wavelet decomposition is termed: indicated runout with wavelet decomposition (IRR-WD), and has not hitherto been reported in the literature. Overall, the method represents a new novel approach for the determination of specific sources of vibration, when used alongside an analytic method as shown in this paper. In the example provided in the paper, the method has been able to pin point

with remarkable accuracy the physical cause of the vibration response. This degree of conformance of the experimental findings with the reported analytical method varies upon the narrowness of the initial frequency range or the chosen "window" and upon the initial sampling rate. It would be fair to state that the results obtained are usually within 5–10% of the analytic predictions for primary bearing-induced vibrations, described in Section 4. For an analytically predicted shaft frequency of 100 Hz, and in the averaging range 95–105 Hz, the repeatable signal is found to correspond to 103.22 Hz. This represents a deviation of 3.22% from the analytical model. Another example corresponds to a calculated shaft frequency of 260 Hz, obtained by IRR-WD's main repeatable component at 257 Hz. This gives deviation from the calculated value by 1.15%. The large number of samples required for higher (or secondary) contributions make the application of IRR-WD quite arduous. To overcome this shortcoming further research is required.

Acknowledgements

The authors wish to express their gratitude to Rye Machine Tools, Buckinghamshire for the donation of some of the experimental facility. The financial assistance of the European Commission under the OPORTO Thematic Network is acknowledged.

Appendix A. Nomenclature

d	nominal ball diameter
D	pitch circle diameter
f_b	ball frequency
f_{bi}	ball to inner race relative speed
f_{b0}	ball to outer race relative speed (ball pass rate)
f_c	cage frequency
f_s	shaft frequency
L	number of equal sector data per revolution
M	number of revolutions
N	number of balls in a bearing
$NRRO$	non-repeatable runout
$TIR(l,m)$	total Indicated Runout
t	time
w	wavelet shape function
α	contact angle

References

[1] C.J. Li, J. Ma, Wavelet decomposition of vibrations for detection of bearing–localized defects, NDT International 30 (3) (1997) 143–149.

[2] F.P. Wardle, Vibration forces produced by waviness of the rolling surfaces of thrust loaded ball bearings, Part 2, experimental validation, Proceedings of the Institute of Mechanical Engineers, Part C: Journal of Mechanical Engineering Science 202 (1988) 313–319.
[3] R. Aini, H. Rahnejat, R. Gohar, An experimental investigation into bearing-induced spindle vibration, Proceedings of the Institute of Mechanical Engineers, Part C: Journal of Mechanical Engineering Science 209 (1995) 107–114.
[4] N. Lynagh, H. Rahnejat, M. Ebrahimi, R. Aini, Bearing induced vibration in precision high speed routing spindles, International Jounal of Machines, Tools and Manufacturing 40 (1999) 561–577.
[5] G. Jang, D. Kim, J.E. Oh, New frequency domain method of non-repeatable runout measurement in a hard disk drive spindle motor, IEEE Transactions on Magnetics 35 (1999) 833–838.
[6] T. Ohmi, Non-repeatable runout of ball –bearing Spindle motor for 2.5″ HDD, IEEE Transactions on Magnetics 32 (1996) 1715–1720.
[7] I. Daubechies, The wavelet transform time–frequency localization and signal analysis, IEEE Transactions on Information Theory 36 (1990) 961–1005.
[8] D.E. Newland, An Introduction to Random Vibrations and Spectral and Wavelet Analysis, 3rd ed., Longman, New York, 1993.
[9] M. Misiti, Y. Misiti, G. Oppenheim, J.M. Poggi, Wavelet Toolbox for Use with The Mathworks, Inc., Natick, MA, 1997.
[10] G. Beylkin, R. Coifman, V. Rokhlin, Fast wavelet transforms and numerical algorithms, Communications on Pure and Applied Mathematics 44 (1991) 141–183.
[11] K. Mathioudakis, Wavelet analysis for gas turbine fault diagnostics, Transactions of the American Society of Mechanical Engineers, Journal of Engineering for Gas Turbines and Power 119 (1997) 870–876.
[12] D.E. Newland, Wavelet analysis of vibration, Part 1: theory, Transactions of the American Society of Mechanical Engineers, Journal of Vibration and Acoustics 116 (1994) 409–416.
[13] D.E. Newland, Wavelet analysis of vibration, Part 2: wavelet maps, Transactions of the American Society of Mechanical Engineers, Journal of Vibration and Acoustics 116 (1994) 417–425.
[14] K. Mori, N. Kasashima, T. Yoshioka, Y. Ueno, Prediction of spalling on a ball bearing by applying the discrete wavelet transform to vibration signals, Wear 195 (1996) 162–168.
[15] S. Mallat, A theory for multi-resolution signal decomposition: the wavelet representation, IEEE Transactions on Pattern Analysis and Machine Intelligence 11 (1989) 674–693.
[16] N. Lynagh, H. Rahnejat, M. Ebrahimi, R. Aini, Diagnostics for real-time vibration monitoring of precision spindles, Proceedings of the Sixth International Symposium, AMST, Institute of Measurement and Control, MEP Publications, Bradford, 1998, pp. 299–310.
[17] H. Rahnejat, R. Gohar, The vibration of radial ball bearings, Proceedings of the Institute of Mechanical Engineers, Part C: Journal of Mechanical Engineering Science 199 (1985) 181–193.
[18] L.D. Meyer, F.F. Ahlgren, B. Weichbrodt, An analytic model for ball bearing vibration to predict vibration response to distributed defects, Transactions of American Society of Mechanical Engineers, Journal of Mechanical Design 102 (1980) 205–210.